THE JOURNAL OF PHYSICAL CHEMISTRY B

Article

Cite This: J. Phys. Chem. B 2018, 122, 7590−7596

pubs.acs.org/JPCB

Frustration vs Prenucleation: Understanding the Surprising Stability of Supersaturated Sodium Thiosulfate Solutions

Judith Reichenbach and Klaas Wynne*

School of Chemistry, University of Glasgow, Glasgow G12 8QQ, U.K.

Supporting Information

ABSTRACT: Gibbs classical nucleation theory predicts that a supersaturated solution will have transient nuclei that flitter in and out of existence. Only when one of these nuclei becomes larger than a critical size, will the solution crystalize. Recently, nonclassical nucleation theories have invoked the presence of prenuclei possibly associated with a liquid−liquid phase separation. However, there are few experimental observations of such prenuclei. Here, we use ultrafast optical Kerr-effect spectroscopy to measure the temperature-dependent low-frequency (sub-gigahertz to terahertz) anisotropic Raman spectra of supersaturated aqueous sodium thiosulfate solutions. Clear evidence of clusters is obtained in the spectra. However, on the basis of the inferred stability of these clusters, it appears that they frustrate rather than promote the formation of crystals. This would explain the surprising stability of supersaturated sodium thiosulfate and similar solutions.

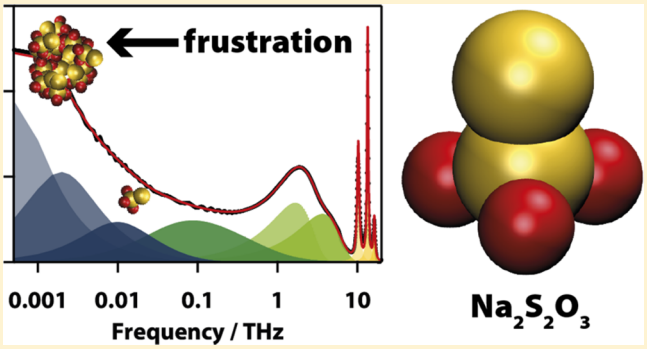

INTRODUCTION

The nucleation of crystals from solutions is critically important in biomineralization, industrial production of pharmaceutical drugs, nanoparticles, and dyes, as well as protein crystallography.[1,2] Gibbs classical nucleation theory describes this process in terms of a process in which single molecules attach or detach from a growing nucleus.[3] Because of competition between a reduction in bulk free energy (scaling with the volume of the nucleus) and an increase in surface tension (scaling with the surface area), nuclei flitter in and out of existence until a nucleus exceeds a critical size and the supersaturated solution crystalizes.

However, the basis of classical nucleation theory has been called into question by a number of studies that showed the presence of thermodynamically stable prenucleation clusters.[4,5] This led to the idea that the critical nucleus might be formed by the addition and removal of clusters rather than molecules.[6] These prenucleation clusters might well be related to a hidden liquid−liquid phase separation critical point that leads to metastable dense liquid as a precursor to crystallization[7−11] and that could even be controlled using external forces.[12] Or alternatively, nucleation might be driven by (oriented) attachments between subcritical clusters that already exhibit a degree of crystallinity.[13]

Another important factor affecting crystal nucleation (or rather the lack thereof) is frustration. Originally proposed by Frank for simple spherical solutes,[14] frustration expresses the idea that, on lowering the temperature to cause supersaturation or supercooling, molecules may assume a packing that locally minimizes the enthalpy but frustrates the formation of the globally minimal free-energy crystalline state.[15] Frustration is the likely basis for supercooling and vitrification and has been associated with liquid−liquid transitions in water and other molecular (supercooled) liquids.[16−21]

Here, we use the ultrafast optical Kerr-effect (OKE) spectroscopy to obtain the low-frequency anisotropic Raman spectra of (supersaturated) solutions.[22] OKE spectroscopy is sensitive to reorientational motions through the anisotropic part of the molecular polarizability tensor.[23,24] The technique has been used to study a wide range of liquids, including ionic liquids,[22,25−30] as well as aqueous solutions of proteins[31,32] and DNA.[33,34] Because the molecular polarizability tensor of water is very nearly isotropic,[35] OKE spectroscopy is ideal for studying the dynamics of solutes in aqueous solution.[36−39]

Sodium thiosulfate pentahydrate yields a supersaturated solution below 49 °C,[40] which is well known to be (meta)stable for weeks and even under significant mechanical perturbation. It is therefore an ideal candidate for the study of frustration and to determine whether frustrated clusters can be observed through OKE spectroscopy. Such clusters would give rise to a slowdown of the orientational-relaxation dynamics and should be easily observable.[37] Furthermore, the recent observation of prenucleation clusters in supersaturated L-(+)-tartaric acid solutions using terahertz spectroscopy suggests that in addition cluster bands may be observed around 1 THz.[41] The thiosulfate ion also has a large

Received: May 1, 2018
Revised: July 6, 2018
Published: July 11, 2018

anisotropic polarizability and is therefore easily distinguished from any water background in OKE spectroscopy.

METHODS

Sample Preparation. Sodium thiosulfate pentahydrate solutions (63.7 wt %, salt/water = 1:5) were made by melting sodium thiosulfate pentahydrate (≥99.5%, Sigma-Aldrich) in a heated ultrasound bath at 65 °C for an hour, followed by cooling to room temperature. Solutions were transferred into 2 mm path length quartz cuvettes (Starna) 1 week after preparation. No crystallization occurred in either the stock solution or the cuvette. A diluted aqueous sodium thiosulfate solution (21.2 wt %, salt/water = 1:32.7) was made by dissolving 0.9930 g of sodium thiosulfate pentahydrate in 2 mL of HPLC gradient grade water (Fisher), which was directly transferred into a 2 mm path length quartz cuvette (Starna).

OKE Experimental Details. The OKE data were taken in purpose-built time-domain pump−probe setups described elsewhere.[31,33] Very briefly, OKE data are taken in an ultrafast pump−probe spectroscopy setup using a Micra laser oscillator (Coherent), yielding laser pulses centered at 800 nm with a pulse width of 20−22 fs, as measured in the sample position, at a repetition rate of 82 MHz. Measurements for pump−probe delays in excess of 20 ps and up to 2 ns were taken with a Legend Elite USX regenerative amplifier (Coherent), which emitted laser pulses with a center wavelength of 800 nm and a repetition rate of 1 kHz. The laser pulses from the latter were recompressed to a pulse width of ∼1 ps with the pulse energy reduced to ∼1 μJ. The maximum delay time of 2 ns resulted in spectral coverage down to 500 MHz in the frequency domain after numerical Fourier transformation. Samples were held in quartz cuvettes inside a temperature-controlled brass block with a precision of ±0.1 °C for measurements at and above 25 °C. For measurements below 25 °C, the cuvettes were placed under a dry nitrogen atmosphere inside a liquid nitrogen-cooled cryostat (Oxford Instruments) with a temperature precision of ±0.1 °C.

OKE Data Analysis. The OKE data for each temperature were averaged, concatenated, and then Fourier-transformed into frequency domain spectra, as described previously.[31,33] Reflective losses from the cryostat windows reduced the signal intensity in the low-temperature spectra. Therefore, all spectra were scaled to the intensity of the 16.2 THz S−S-stretch vibrational mode, which was found to exhibit no appreciable intensity change with temperature. The contribution of water to the OKE spectrum scales, of course with the amount of water present, made it non-negligible only in the 1:32.7 solution (see Figure 1). A parameterized water OKE spectrum[33] scaled with the water weight-fraction was therefore used in the 1:32.7 solution fit. The spectra were fitted with a combination of Brownian oscillators, antisymmetrized Gaussians, and variations of the Havriliak−Negami function, which has previously been shown to yield a good empirical model for describing the molecular dynamics in liquids.[22] The temperature-dependent spectra were fitted sequentially by altering the fit parameters used for the preceding temperature. To achieve a stable fit, this was done both from the low-temperature and high-temperature end and functions were added or taken away as dictated by the data.

The definitions for the fit functions used here are,[22] for the Brownian oscillator

$$B(\omega) = \mathrm{Im}\, A_B\omega_0^2/(\omega_0^2 - \omega(\omega + 2i\gamma))$$

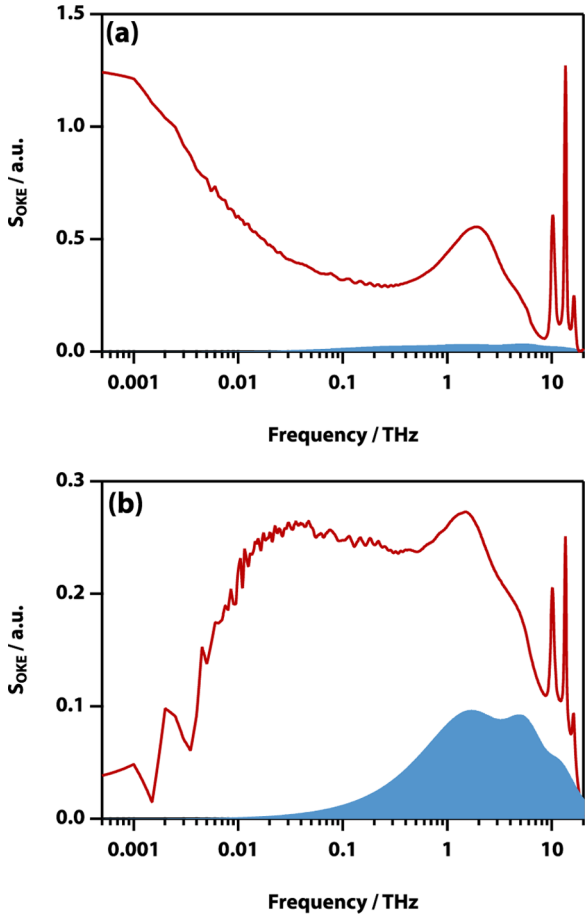

Figure 1. Comparison of calculated water content for (a) the 1:5 solution and (b) the 1:32.7 solution. Shown are the OKE spectra of the solution (red lines) and the calculated water fit (blue area fill). It can be seen that the water contribution in the 1:5 solution (a) is roughly an order of magnitude smaller than the intensity in the 1 THz region, whereas the difference is only a factor of about three for the 1:32.7 solution (b).

with amplitude A_B, undamped oscillator angular frequency ω_0, and damping rate γ, and were used to model intramolecular vibrations in the spectra. For librations, antisymmetrized Gaussians were used, which are defined as

$$\mathrm{ASG}(\omega) = A_{\mathrm{ASG}}\left(\exp\left(\frac{-(\omega - \omega_0)^2}{\gamma^2}\right) - \exp\left(\frac{-(\omega + \omega_0)^2}{\gamma^2}\right)\right)$$

where A_{ASG} stands for the amplitude. Finally, the Havriliak−Negami function was defined as

$$H_{\alpha,\beta}(\omega) = \frac{A_{\mathrm{HN}}}{(1 + (-i\omega\tau)^{\alpha})^{\beta}}$$

with the amplitude A_{HN} and the relaxation time τ. Here, α and β are broadening and asymmetry parameters, respectively, which take on values between 0 and 1. Restraints on α and β denote special cases of the Havriliak−Negami function. In the case of $\beta = 1$, the Havriliak−Negami function is reduced to a Cole−Cole function, which is used to model cage rattling and cage diffusion processes associated with β-relaxation. Orienta-

DOI: 10.1021/acs.jpcb.8b04112
J. Phys. Chem. B 2018, 122, 7590−7596

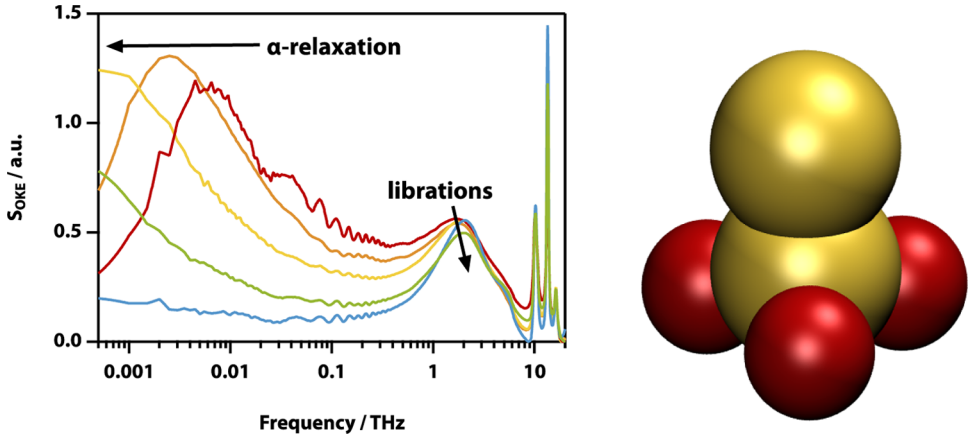

Figure 2. Temperature dependence for the OKE spectra of the 1:5 solution. (Left) The spectra are shown with a logarithmic frequency and a linear intensity axis for 75 to −25 °C (red to blue, in direction of the arrows). It can be seen that the α-relaxation shifts to lower frequency upon cooling, whereas the librations shift to slightly higher frequencies. (Right) Three-dimensional molecular structure of the thiosulfate anion.

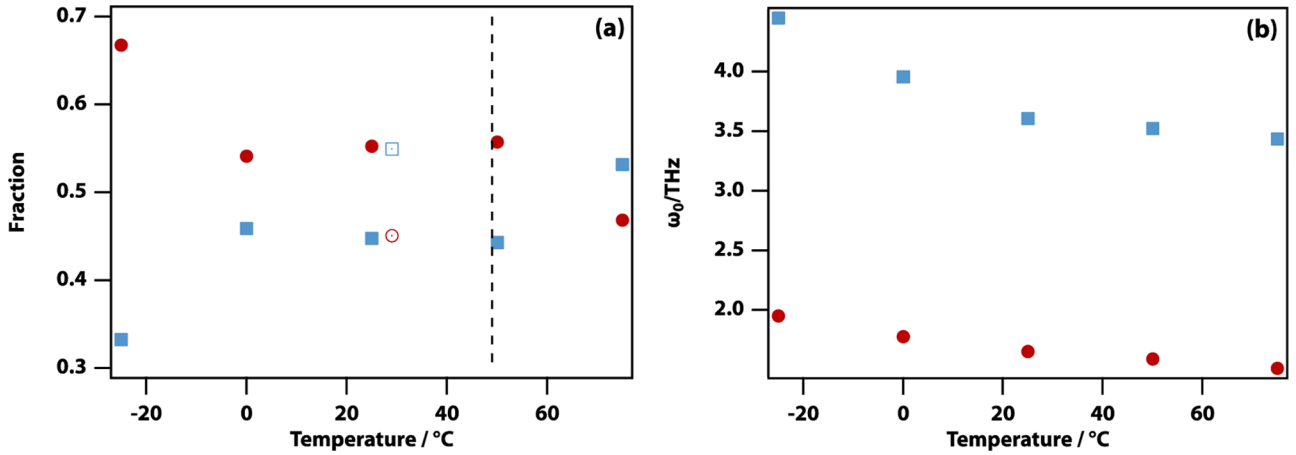

Figure 3. Temperature dependence of the fit parameters of the librational modes for the 1:5 solution. (a) The amplitudes of the two librational components. Red solid circles denote the fraction of the lower frequency libration G1, whereas blue solid squares denote the fraction of the higher frequency shoulder G2. The amplitudes of the 1:32.7 solution at 25 °C are shown as a red empty circle and blue square displaced to 30 °C for clarity. The vertical dashed line indicates the supersaturation temperature (49 °C) (b) the librational frequency ω_0 of the two librational components.

tional relaxation associated with α-relaxation is modeled here by Debye functions (corresponding to an exponential decay in the time domain) and is described by Havriliak−Negami functions with both α and β held at 1.

If only a single orientational-relaxation time characterizes the system, one Debye function is sufficient to model the α-relaxation. In the samples studied here, however, a broadened α-relaxation band was found, which was modeled by a distribution of Debye functions wherever possible to yield distributions of relaxation times. If the experimental α-relaxation band was not sufficiently defined to allow fitting with a distribution of Debye functions, a Cole−Davidson function was used instead. For a Cole−Davidson function, α is held at 1 and the function is asymmetrically broadened compared to a Debye function, with a less steep slope on the high-frequency side.

To extract meaningful relaxation-time distributions from the α-relaxation, the shape of the fit functions is important. Therefore, a modified version of the Havriliak−Negami function was used to address unphysical behavior in which intermediate time scale diffusive relaxation (β-relaxation) is either faster than librations or slower than α-relaxation. In short, the modifications prevent an instantaneous rise in the time domain before the relaxation (instead rising with rate Γ_{rise}) and terminate the decay once the next relaxational process begins (with rate Γ_{decay}), allowing for sequential relaxation.[22] Sequential relaxation is the concept that the dynamics in liquids depend on structures, which are sequentially destroyed as different relaxation mechanisms set in.

RESULTS

The temperature-dependent spectra of the 1:5 solution are shown in Figure 2. They feature vibrational peaks above 10 THz, librational bands around 2 THz, as well as the α-relaxation band below 100 GHz, and the β-relaxation band between the librations and the α-relaxation. The positions of the vibrational bands at 10.2, 13.4, and 16.2 THz (306, 402, and 488 cm^{-1}) have been shown to be concentration-independent,[42,43] and no significant temperature dependence was observed here in the 1:5 solution spectra. On the other side of the frequency scale, the α-relaxation band shows a shift toward lower frequencies with decreasing temperature. This is a common observation, as molecular movement tends to be

DOI: 10.1021/acs.jpcb.8b04112
J. Phys. Chem. B 2018, 122, 7590−7596

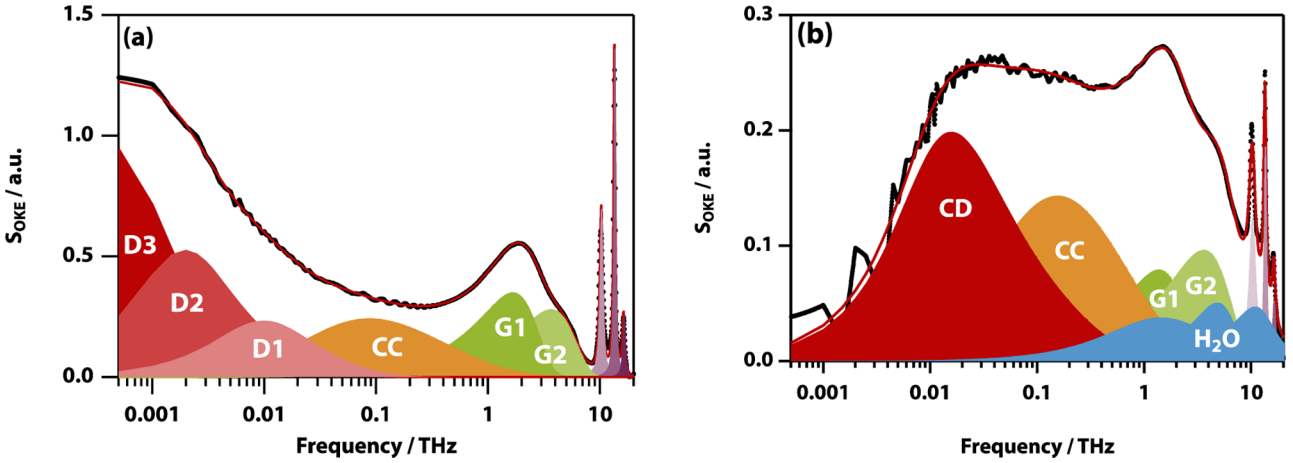

Figure 4. Fits for the OKE spectra at 25 °C of (a) the 1:5 solution and (b) the 1:32.7 solution. Shown are the vibrational modes (purple), the librational modes G1 and G2 (green), the β-relaxation CC (orange), and the α-relaxation (red), which are labeled as D1−D3 or CD for (a) and (b), respectively. Featured in (b) is the calculated water contribution of the spectrum (blue), which is labeled as H_2O.

Table 1. Relaxation Times and Calculated Volumes for the 1:5 and 1:32.7 Solutions[a]

viscosities[46,47]	0 °C 1:5	25 °C 1:5	50 °C 1:5	75 °C 1:5	25 °C 1:32.7
η_{H_2O}/mPa s	1.79	0.89	0.55	0.38	0.89
η_{Sol}/mPa s	547.55	70.12	20.72	9.25	1.85
times and volumes	0 °C 1:5	25 °C 1:5	50 °C 1:5	75 °C 1:5	25 °C 1:32.7
τ_{D1}/ps		99.6	45.4	25.4	87.0
V_{D1,H_2O}/Å^3		460.5	370.6	323.7	402.4
$V_{D1,Sol}$/Å^3		5.9	9.8	13.2	193.5
τ_{D2}/ps		510.5	210.0		
V_{D2,H_2O}/Å^3		2361.1	1714.1		
$V_{D2,Sol}$/Å^3		30.0	45.2		
τ_{D3}/ps	5101.6	2201.9	704.7	206.7	
V_{D3,H_2O}/Å^3	10 741.6	10 184.1	5752.9	2632.9	
$V_{D3,Sol}$/Å^3	35.1	129.3	151.7	107.5	

[a]Included are the viscosities used for the calculations, η_{H_2O} for water and η_{Sol} for the solution.

slower at lower temperatures (higher viscosity), leading to longer relaxation times. The band also exhibits significant broadening, which made it impossible to fit the data with only a single Debye function (see below).

The librational band, meanwhile, showed a peak (G1) as well as a shoulder (G2), which indicates two distinct librational modes. Thiosulfate, however, is trigonal bipyramidal, as seen in Figure 2. This means that from symmetry considerations, only one librational band should be visible. Considering three inertial axes, one in line with the two sulfur atoms and two perpendicular to them, the libration about the sulfur axis would be invisible in the OKE spectrum, whereas the other two librations would be degenerate. Therefore, the data demonstrate that two distinguishable types of thiosulfate ions must exist in the solution, differentiated by different environments. Figure 3a plots the temperature-dependent fractional amplitudes of these two librational components. Although the high-frequency component (G2) is larger when the sample is undersaturated (75 °C), the low-frequency component is larger when supersaturated and dominates at the lowest temperature (−25 °C).

Also shown are the temperature-dependent (undamped) frequencies of the librations, which increase slightly on cooling (Figure 3b). This can be understood as a consequence of the lower density at higher temperatures, which manifests itself in a shallower intermolecular potential.[44]

Figure 4 compares the 1:5 solution spectrum at 25 °C with a less concentrated 1:32.7 solution at the same temperature. The librations of the 1:5 solution are found at higher frequencies than those of the 1:32.7 solutions, whereas the α-relaxation can be found at lower frequencies. This mirrors the behavior of the temperature dependence, where the librational band moved to higher frequencies and the α-relaxation band moved to lower frequencies upon cooling. As a result, the 1:32.7 solution spectrum shows more similarity to the high-temperature 1:5 solution spectra than the 25 °C 1:5 solution spectrum. This can be seen clearly for the fractional amplitudes of the 1:32.7 solutions shown in Figure 3a, which have the same ordering of magnitude as that of the undersaturated 1:5 solution.

The α-relaxation bands seen in the spectra in Figure 4 are significantly broadened and cannot be fit with a single Debye function. In the OKE spectrum of the 1:5 solution, we can clearly distinguish a distribution of relaxation times that is well represented by three separate Debye functions with relaxation times of 99.6, 510, and 2.2 ns (see Table 1). The OKE spectrum of the 1:32.7 solution is relatively noisy below 100 GHz. However, to fit the data on the low-frequency end, an asymmetric Cole−Davidson function is required, also indicating a range of α-relaxation times.

DOI: 10.1021/acs.jpcb.8b04112
J. Phys. Chem. B 2018, 122, 7590−7596

DISCUSSION

The observed shifts in the librational and orientational-relaxation bands are in line with the behavior usually observed in aqueous solutions.[45] The two librational bands, meanwhile, cannot be accounted for by symmetry considerations and demonstrate the existence of two different environments for the thiosulfate ions. In all liquids except water, the librational band is observed to peak at a frequency of a few terahertz.[22,37] Thus, the "shoulder" labeled G2 most likely corresponds to librations of thiosulfate in aqueous solution. This is consistent with this band having the largest amplitude both in the 1:5 solution at high temperature and the 1:32.7 solution, both of which are undersaturated. The lower frequency G1 band, then, most likely corresponds with librations in a cluster. This is consistent with the G1 fraction increasing on cooling into the supersaturated regime. Thus, the amplitudes of the librational bands are consistent with the formation of clusters under supersaturation.

This effect of clustering on lowering the temperature is also seen by the broadening of the α-relaxation band in these samples. The orientational-relaxation time can be related to the volume of the object that is being observed using the Stokes–Einstein–Debye (SED) relation. The orientational diffusion coefficient is given by $D_{rot} = k_B T/6\eta V$, where V is the object's volume and η is the shear viscosity. The rotational diffusion coefficient can be related to the orientational-relaxation time, as observed in OKE through $\tau = (6D_{rot})^{-1}$. The SED expression works fine for the dilute 1:32.7 solution: using the measured relaxation time and viscosity, a volume of 193.5 Å^3 is found, which compares well with the molecular volume of thiosulfate of 147 Å^3 (estimated from the density and molar mass of the anhydrous crystal). The slightly increased value (slower relaxation) indicates a degree of clustering consistent with the requirement for fitting the data with a Cole–Davidson function. In addition, there is no evidence for fractional SED behavior for the thiosulfate anion in water.[37]

However, the SED equation completely fails for the supersaturated 1:5 solutions. Using known values of the shear viscosity of the solution[46,47] yields extremely low volumes, as low as 5.9 Å^3, corresponding to anomalously fast relaxation. Such decoupling of rotational relaxation from the solution viscosity was observed previously[48] and is associated with the "mayonnaise effect":[49] clustering and structuring in (aqueous salt) solutions lead to a nonlinear increase in bulk viscosity through the presence of a jamming transition[50−52] at a critical concentration. However, solutes orientationally relaxing in such an anomalously viscous solution only sense their immediate environment, which in this case is water.

Therefore, the SED calculations should be carried out using the (temperature-dependent) viscosity of water. This leads to much more reasonable volumes ranging from dimers to clusters of 73 thiosulfate ions in the 1:5 solution at 0 °C, whereas the 1:32.7 solution showed a distribution consisting of mainly trimers (see Table 1). The orientational relaxation in the 1:5 solution at −25 °C is too slow to be measured in our OKE setup but is certainly much slower than 4 ns, corresponding to cluster sizes well in excess of 100.

CONCLUSIONS

Thus, the data presented here are consistent with the presence of clusters ranging from trimers to more than 100 anions (and presumably the sodium counterions that are invisible in these OKE experiments). The fact that distinct bands are observed down to 500 MHz (the limit of our setup) implies that the lifetime of these clusters must be well in excess of 2 ns. The clustering is associated with a lowering of the librational frequency of the thiosulfate ion. The characteristic translational diffusion length scale for thiosulfate in water is ∼2 nm on this timescale. This suggests that the observed clusters are not prenucleation clusters (which are expected to flicker in and out of existence) but stable clusters frustrating the formation of the thermodynamically most stable crystalline state. Such frustration effects are well established in glass-forming supercooled liquids but somewhat unexpected in much more dilute solutions. The presence of frustrating clusters in sodium thiosulfate pentahydrate explains the unusual stability (over more than weeks) of the supersaturated solution and similarly stable supersaturated solutions.

ASSOCIATED CONTENT

Supporting Information

The Supporting Information is available free of charge on the ACS Publications website at DOI: 10.1021/acs.jpcb.8b04112.

Fit parameters for the 1:5 aqueous sodium thiosulfate solution; fit parameters for the 1:32.7 aqueous sodium thiosulfate solution; fitted spectra for the 1:5 aqueous sodium thiosulfate solution (PDF)

Accession Codes

The OKE data that support the findings of this study are available in Enlighten: Research Data Repository (University of Glasgow) with the identifier: http://dx.doi.org/10.5525/gla.researchdata.636.

AUTHOR INFORMATION

Corresponding Author

*E-mail: klaas.wynne@glasgow.ac.uk. Phone: +44 141 330 8522.

ORCID

Klaas Wynne: 0000-0002-5305-5940

Notes

The authors declare no competing financial interest.

ACKNOWLEDGMENTS

We acknowledge the Engineering and Physical Sciences Research Council (EPSRC) for support through grants EP/J009733/1, EP/K034995/1, EP/N508792/1, and EP/N007417/1.

REFERENCES

(1) Davey, R. J.; Schroeder, S. L. M.; ter Horst, J. H. Nucleation of organic crystals–a molecular perspective. *Angew. Chem., Int. Ed.* **2013**, *52*, 2166–2179.

(2) Bučar, D.-K.; Lancaster, R. W.; Bernstein, J. Disappearing Polymorphs Revisited. *Angew. Chem., Int. Ed.* **2015**, *54*, 6972–6993.

(3) Erdemir, D.; Lee, A. Y.; Myerson, A. S. Nucleation of Crystals from Solution: Classical and Two-Step Models. *Acc. Chem. Res.* **2009**, *42*, 621–629.

(4) Gebauer, D.; Voelkel, A.; Coelfen, H. Stable Prenucleation Calcium Carbonate Clusters. *Science* **2008**, *322*, 1819–1822.

(5) Demichelis, R.; Raiteri, P.; Gale, J. D.; Quigley, D.; Gebauer, D. Stable prenucleation mineral clusters are liquid-like ionic polymers. *Nat. Commun.* **2011**, *2*, No. 590.

(6) De Yoreo, J. J.; Gilbert, P. U. P. A.; Sommerdijk, N. A. J. M.; Penn, R. L.; Whitelam, S.; Joester, D.; Zhang, H.; Rimer, J. D.; Navrotsky, A.; Banfield, J. F.; et al. Crystallization by particle

DOI: 10.1021/acs.jpcb.8b04112
J. Phys. Chem. B 2018, 122, 7590–7596

attachment in synthetic, biogenic, and geologic environments. *Science* **2015**, *349*, No. aaa6760.
(7) ten Wolde, P. R.; Frenkel, D. Enhancement of protein crystal nucleation by critical density fluctuations. *Science* **1997**, *277*, 1975−1978.
(8) Wallace, A. F.; Hedges, L. O.; Fernandez-Martinez, A.; Raiteri, P.; Gale, J. D.; Waychunas, G. A.; Whitelam, S.; Banfield, J. F.; De Yoreo, J. J. Microscopic evidence for liquid-liquid separation in supersaturated CaCO3 solutions. *Science* **2013**, *341*, 885−889.
(9) Gebauer, D.; Kellermeier, M.; Gale, J. D.; Bergström, L.; Cölfen, H. Pre-nucleation clusters as solute precursors in crystallisation. *Chem. Soc. Rev.* **2014**, *43*, 2348−2371.
(10) Mosses, J.; Turton, D. A.; Lue, L.; Sefcik, J.; Wynne, K. Crystal templating through liquid-liquid phase separation. *Chem. Commun.* **2015**, *51*, 1139−1142.
(11) Smeets, P. J. M.; Finney, A. R.; Habraken, W. J. E. M.; Nudelman, F.; Friedrich, H.; Laven, J.; De Yoreo, J. J.; Rodger, P. M.; Sommerdijk, N. A. J. M. A classical view on nonclassical nucleation. *Proc. Natl. Acad. Sci. U.S.A.* **2017**, *114*, E7882−E7890.
(12) Walton, F.; Wynne, K. Control over phase separation and nucleation using a laser-tweezing potential. *Nat. Chem.* **2018**, *10*, 506−510.
(13) Van Driessche, A. E. S.; Van Gerven, N.; Bomans, P. H. H.; Joosten, R. R. M.; Friedrich, H.; Gil-Carton, D.; Sommerdijk, N. A. J. M.; Sleutel, M. Molecular nucleation mechanisms and control strategies for crystal polymorph selection. *Nature* **2018**, *556*, 89−94.
(14) Frank, F. C. Supercooling of liquids. *Proc. R. Soc. A* **1952**, *215*, 43−46.
(15) Keen, D. A.; Goodwin, A. L. The crystallography of correlated disorder. *Nature* **2015**, *521*, 303−309.
(16) Murata, K.-I.; Tanaka, H. Microscopic identification of the order parameter governing liquid−liquid transition in a molecular liquid. *Proc. Natl. Acad. Sci. U.S.A.* **2015**, *112*, 5956−5961.
(17) Mosses, J.; Syme, C. D.; Wynne, K. Order Parameter of the Liquid−Liquid Transition in a Molecular Liquid. *J. Phys. Chem. Lett.* **2015**, *6*, 38−43.
(18) Gallo, P.; Amann-Winkel, K.; Angell, C. A.; Anisimov, M. A.; Caupin, F.; Chakravarty, C.; Lascaris, E.; Loerting, T.; Panagiotopoulos, A. Z.; Russo, J.; et al. Water: A Tale of Two Liquids. *Chem. Rev.* **2016**, *116*, 7463−7500.
(19) Syme, C. D.; Mosses, J.; González Jiménez, M.; Shebanova, O.; Walton, F.; Wynne, K. Frustration of crystallisation by a liquid−crystal phase. *Sci. Rep.* **2017**, *7*, No. 42439.
(20) Russo, J.; Tanaka, H. Understanding water's anomalies with locally favoured structures. *Nat. Commun.* **2014**, *5*, No. 3556.
(21) Woutersen, S.; Ensing, B.; Hilbers, M.; Zhao, Z.; Angell, C. A. A liquid-liquid transition in supercooled aqueous solution related to the HDA-LDA transition. *Science* **2018**, *359*, 1127−1131.
(22) Reichenbach, J.; Ruddell, S. A.; González Jiménez, M.; Lemes, J.; Turton, D. A.; France, D. J.; Wynne, K. Phonon-like Hydrogen-Bond Modes in Protic Ionic Liquids. *J. Am. Chem. Soc.* **2017**, *139*, 7160−7163.
(23) Fecko, C.; Eaves, J.; Tokmakoff, A. Isotropic and anisotropic Raman scattering from molecular liquids measured by spatially masked optical Kerr effect spectroscopy. *J. Chem. Phys.* **2002**, *117*, 1139−1154.
(24) Hunt, N. T.; Jaye, A. A.; Meech, S. R. Ultrafast dynamics in complex fluids observed through the ultrafast optically-heterodyne-detected optical-Kerr-effect (OHD-OKE). *Phys. Chem. Chem. Phys.* **2007**, *9*, 2167−2180.
(25) Lynden-Bell, R. M.; Xue, L.; Tamas, G.; Quitevis, E. L. Local structure and intermolecular dynamics of an equimolar benzene and 1,3-dimethylimidazolium bis[(trifluoromethane)sulfonyl]amide mixture: Molecular dynamics simulations and OKE spectroscopic measurements. *J. Chem. Phys.* **2014**, *141*, No. 044506.
(26) Kakinuma, S.; Shirota, H. Dynamic Kerr Effect Study on Six-Membered-Ring Molecular Liquids: Benzene, 1,3-Cyclohexadiene, 1,4-Cyclohexadiene, Cyclohexene, and Cyclohexane. *J. Phys. Chem. B* **2015**, *119*, 4713−4724.
(27) Taschin, A.; Bartolini, P.; Marcelli, A.; Righini, R.; Torre, R. Supercooling and freezing processes in nanoconfined water by time-resolved optical Kerr effect spectroscopy. *J. Phys.: Condens. Matter* **2015**, *27*, No. 194107.
(28) Perakis, F.; Marco, L. D.; Shalit, A.; Tang, F.; Kann, Z. R.; Kühne, T. D.; Torre, R.; Bonn, M.; Nagata, Y. Vibrational Spectroscopy and Dynamics of Water. *Chem. Rev.* **2016**, *116*, 7590−7607.
(29) Bailey, H. E.; Wang, Y.-L.; Fayer, M. D. Impact of Hydrogen Bonding on the Dynamics and Structure of Protic Ionic Liquid/Water Binary Mixtures. *J. Phys. Chem. B* **2017**, *121*, 8564−8576.
(30) Kampfrath, T.; Campen, R. K.; Wolf, M.; Sajadi, M. The Nature of the Dielectric Response of Methanol Revealed by the Terahertz Kerr Effect. *J. Phys. Chem. Lett.* **2018**, *9*, 1279−1283.
(31) Turton, D. A.; Senn, H. M.; Harwood, T.; Lapthorn, A. J.; Ellis, E. M.; Wynne, K. Terahertz underdamped vibrational motion governs protein-ligand binding in solution. *Nat. Commun.* **2014**, *5*, No. 3999.
(32) Mazur, K.; Heisler, I. A.; Meech, S. R. Water dynamics at protein interfaces: ultrafast optical Kerr effect study. *J. Phys. Chem. A* **2012**, *116*, 2678−2685.
(33) González Jiménez, M.; Ramakrishnan, G.; Harwood, T.; Lapthorn, A. J.; Kelly, S. M.; Ellis, E. M.; Wynne, K. Observation of coherent delocalized phonon-like modes in DNA under physiological conditions. *Nat. Commun.* **2016**, *7*, No. 11799.
(34) Hithell, G.; González-Jiménez, M.; Greetham, G. M.; Donaldson, P. M.; Towrie, M.; Parker, A. W.; Burley, G. A.; Wynne, K.; Hunt, N. T. Ultrafast 2D-IR and optical Kerr effect spectroscopy reveal the impact of duplex melting on the structural dynamics of DNA. *Phys. Chem. Chem. Phys.* **2017**, *19*, 10333−10342.
(35) Murphy, W. Rayleigh depolarization ratio and rotational Raman-spectrum of water-vapor and polarizability components for water molecule. *J. Chem. Phys.* **1977**, *67*, 5877−5882.
(36) Ramakrishnan, G.; González Jiménez, M.; Lapthorn, A. J.; Wynne, K. The Spectrum of Slow and Super-Slow (Picosecond to Nanosecond) Water Dynamics around Organic and Biological Solutes. *J. Phys. Chem. Lett.* **2017**, *8*, 2964−2970.
(37) Turton, D. A.; Wynne, K. Stokes−Einstein−Debye Failure in Molecular Orientational Diffusion: Exception or Rule? *J. Phys. Chem. B* **2014**, *118*, 4600−4604.
(38) Heisler, I. A.; Mazur, K.; Yamaguchi, S.; Tominaga, K.; Meech, S. R. Measuring acetic acid dimer modes by ultrafast time-domain Raman spectroscopy. *Phys. Chem. Chem. Phys.* **2011**, *13*, 15573−15579.
(39) Mazur, K.; Heisler, I. A.; Meech, S. R. THz Spectra and Dynamics of Aqueous Solutions Studied by the Ultrafast Optical Kerr Effect. *J. Phys. Chem. B* **2011**, *115*, 2563−2573.
(40) Young, S. W.; Mitchell, J. P. A study of the supercooled fusions and solutions of sodium thiosulphate. *J. Am. Chem. Soc.* **1904**, *26*, 1389−1413.
(41) Soltani, A.; Gebauer, D.; Duschek, L.; Fischer, B. M.; Cölfen, H.; Koch, M. Crystallization Caught in the Act with Terahertz Spectroscopy: Non-Classical Pathway for l-(+)-Tartaric Acid. *Chem. - Eur. J.* **2017**, *23*, 14128−14132.
(42) Haigh, J. A.; Hendra, P. J.; Rowlands, A. J.; Degen, I. A.; Newman, G. A. Raman spectroscopy of thiosulphates. *Spectrochim. Acta, Part A* **1993**, *49*, 723−725.
(43) von Siebert, H. Kraftkonstante und Strukturchemie. V. Struktur der Sauerstoffsäuren. *Z. Anorg. Allg. Chem.* **1954**, *275*, 225−240.
(44) Czurlok, D.; Gleim, J.; Lindner, J.; Vöhringer, P. Vibrational Energy Relaxation of Thiocyanate Ions in Liquid-to-Supercritical Light and Heavy Water. A Fermi's Golden Rule Analysis. *J. Phys. Chem. Lett.* **2014**, *5*, 3373−3379.
(45) Turton, D. A.; Hunger, J.; Stoppa, A.; Thoman, A.; Candelaresi, M.; Hefter, G.; Walther, M.; Buchner, R.; Wynne, K. Rattling the cage: Micro- to mesoscopic structure in liquids as simple as argon and as complicated as water. *J. Mol. Liq.* **2011**, *159*, 2−8.
(46) Bhattacharjee, C.; Ismail, S.; Ismail, K. Density and viscosity of sodium thiosulfate pentahydrate (Na2S2O3.cntdot.5H2O) + potassium nitrate melt. *J. Chem. Eng. Data* **1986**, *31*, 117−118.

DOI: 10.1021/acs.jpcb.8b04112
J. Phys. Chem. B 2018, 122, 7590−7596

(47) Mahiuddin, S.; Ismail, K. Temperature and concentration dependence of the viscosity of aqueous sodium nitrate and sodium thiosulphate electrolytic systems. *Fluid Phase Equilib.* **1996**, *123*, 231−243.
(48) Turton, D. A.; Hunger, J.; Hefter, G.; Buchner, R.; Wynne, K. Glasslike behavior in aqueous electrolyte solutions. *J. Chem. Phys.* **2008**, *128*, No. 161102.
(49) Wynne, K. The Mayonnaise Effect. *J. Phys. Chem. Lett.* **2017**, *8*, 6189−6192.
(50) Liu, A.; Nagel, S. Nonlinear dynamics - Jamming is not just cool any more. *Nature* **1998**, *396*, 21−22.
(51) Zhang, Z.; Xu, N.; Chen, D. T. N.; Yunker, P.; Alsayed, A. M.; Aptowicz, K. B.; Habdas, P.; Liu, A. J.; Nagel, S. R.; Yodh, A. G. Thermal vestige of the zero-temperature jamming transition. *Nature* **2009**, *459*, 230−233.
(52) Mari, R.; Krzakala, F.; Kurchan, J. Jamming versus Glass Transitions. *Phys. Rev. Lett.* **2009**, *103*, No. 025701.

DOI: 10.1021/acs.jpcb.8b04112
J. Phys. Chem. B 2018, 122, 7590−7596